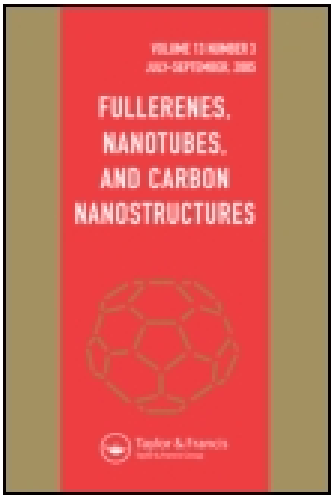

Fullerenes, Nanotubes and Carbon Nanostructures
Publication details, including instructions for authors and subscription information:
http://www.tandfonline.com/loi/lfnn20

Multi-walled Carbon Nanotube Conductivity Enhancement and Band Gap Widening via Rapid Pulsed Thermal Annealing

M. T. Cole [a] , J. T. H. Tsai [b] , Y. T. Chiao [b] , C. Li [b] & Y. Zhang [b]
[a] Electronic Devices and Materials, Centre for Advanced Photonics & Electronics , University of Cambridge , UK
[b] Institute of Optoelectronic Sciences, National Taiwan Ocean University , Keelung , Taiwan
Accepted author version posted online: 02 Dec 2013.Published online: 05 Mar 2014.

To cite this article: M. T. Cole , J. T. H. Tsai , Y. T. Chiao , C. Li & Y. Zhang (2014) Multi-walled Carbon Nanotube Conductivity Enhancement and Band Gap Widening via Rapid Pulsed Thermal Annealing, Fullerenes, Nanotubes and Carbon Nanostructures, 22:6, 545-554, DOI: 10.1080/1536383X.2012.702154

To link to this article: http://dx.doi.org/10.1080/1536383X.2012.702154

Fullerenes, Nanotubes, and Carbon Nanostructures, 22: 545–554, 2014

ISSN: 1536-383X print / 1536-4046 online
DOI: 10.1080/1536383X.2012.702154

Taylor & Francis
Taylor & Francis Group

Multi-walled Carbon Nanotube Conductivity Enhancement and Band Gap Widening via Rapid Pulsed Thermal Annealing

M. T. COLE[1], J. T. H. TSAI[2], Y. T. CHIAO[2], C. LI[2] AND Y. ZHANG[2]

[1]Electronic Devices and Materials, Centre for Advanced Photonics & Electronics, University of Cambridge, UK
[2]Institute of Optoelectronic Sciences, National Taiwan Ocean University, Keelung, Taiwan

Herein we report on the transport characteristics of rapid pulsed vacuum-arc thermally annealed, individual and network multi-walled carbon nanotubes. Substantially reduced defect densities (by at least an order of magnitude), measured by micro-Raman spectroscopy, and were achieved by partial reconstruction of the bamboo-type defects during thermal pulsing compared with more traditional single-pulse thermal annealing. Rapid pulsed annealed processed networks and individual multi-walled nanotubes showed a consistent increase in conductivity (of over a factor of five at room temperature), attributed to the reduced number density of resistive axial interfaces and, in the case of network samples, the possible formation of structural bonds between crossed nanotubes. Compared to the highly defective as-grown nanotubes, the pulsed annealed samples exhibited reduced temperature sensitivity in their transport characteristics signifying the dominance of scattering events from structural defects. Transport measurements in the annealed multi-walled nanotubes deviated from linear Ohmic, typically metallic, behavior to an increasingly semiconducting-like behavior attributed to thermally induced axial strains. Rapid pulsed annealed networks had an estimated band gap of 11.26 meV (as-grown; 6.17 meV), and this observed band gap enhancement was inherently more pronounced for individual nanotubes compared with the networks most likely attributed to mechanical pinning effect of the probing electrodes which possibly amplifies the strain induced band gap. In all instances the estimated room temperature band gaps increased by a factor of two. The gating performance of back-gated thin-film transistor structures verified that the observed weak semiconductivity (p-type) inferred from the transport characteristic at room temperature.

Keywords Multi-walled carbon nanotubes, pulsed annealing, semiconductivity, recrystallization

Introduction

Carbon nanotubes (CNTs) have been thrust to the forefront of materials science due to their unique electrical, optical, and mechanical proprieties as well as their versatility in

Address correspondence to J. T. H. Tsai, PhD, Electronic Devices & Materials, Centre for Advanced Photonics & Electronics, 9 JJ Thomson Avenue, University of Cambridge, CB3 0FA, UK. E-mail: mtc35@cam.ac.uk

Color versions of one or more of the figures in the article can be found online at www.tandfonline.com/lfnn.

a variety of applications demanding flexibility and optical transparency (1). CNTs, one-dimensional, high aspect ratio allotropes of carbon can be classified into two groups: single-walled CNTs (SWCNTs) and multi-walled CNTs (MWCNTs). SWCNTs can be either metallic or semiconducting (2–5), a desirable binary characteristic based on the crystallographic structure of the CNTs. CNTs have been successfully employed as the active material in many electronic applications, including low-dimensional nanostructured field-effect transistors (FETs) (6,7) and conducting composite networks (8,9). Polymer-CNT composites are mechanically robust (high Young's modulus, stiffness, and flexibility) and highly conductive. In such applications it is imperative that the CNT networks have as high an electrical conductivity as possible, achieved by exceeding the percolation threshold, in order to achieve isotropic charge transfer. Somewhat counter intuitively, however, is that the maximum conductivity within these composites can be achieved with relatively low CNT wt%, typically of the order of 0.05wt% (9,10). Enhancing the conductivity of composite materials cannot be achieved by simply increasing the CNT content alone. Increasing the wt% often results in CNT bundling and/or aggregation during the polymer cure, which substantially degrades the network conductance and charge transfer isotropy.

For CNTs the degree of crystallinity of the graphitic sidewalls is intimately related to the CNTs physically observable properties—arguably most important of which is the CNTs conductivity. High temperature synthesis techniques ($\sim$2800^{o}C), such as arc discharge deposition, produce highly graphitic and consequently highly conductive CNTs due to the reduced density of scatter sites. Nonetheless, these high-quality CNTs are combined with large amounts of undesirable carbonaceous by-products such as buckminsterfullerenes, diamond-like carbon and amorphous carbon. Such carbon species can only be partly removed by *chemi douche* techniques, which themselves degrade the high-quality as-grown CNTs through aggressive ultrasonication and acid treatments. As-grown MWCNTs invariably exhibit an assortment of structural defects. Most defects observed for low temperature synthesis techniques such as plasma enhanced chemical vapor deposition (PE-CVD, $\sim$700^{o}C) are bamboo facets (Figure 1a). Such defects are a result of the inhibited graphitization due to the relatively low growth temperatures and residual N_2 encapsulation (11). Wet chemistry processes have yet to show efficient defect removal. An effective alternative route to drastically reduce defect densities is via modest temperature rapid pulsed vacuum-arc thermal annealed (RTA) processing. Our previous micro-Raman spectroscopy studies (12,13) established that the defect density in RTA processed MWCNTs is heavily reduced by pulsing the thermal treatment (14). Defect removal was enhanced by the pulsed nature of the process compared with more traditional single pulse annealing. In this paper we report on our continuing work on probing the electronic transport characteristics of these rapid pulsed spark-annealed thermally treated individual and networked MWCNTs.

Structurally defective CNTs have considerably reduced electrical conductivity (14). Point defects in the hexagonal C-C lattice of the CNTs side-walls function as electron scattering sites. Conductivities can be substantially enhanced through heat treatment and annealing processes. Improving our understanding of the effects of thermal treatments on individual, and networks of, MWCNTs will ultimately facilitate enhanced engineered composites and nanostructured networks. Individual MWCNTs have been considered in an attempt to elucidate the global versus local effects of our rapid thermal pretreatment process. Is the observed conductivity enhancement attributed to graphitization in the individual MWCNTs or simply enhanced connectivity within the entire network? Such enhanced connectivity may be achieved by thermal adjustments to the inter-tube potential barriers, by removing weakly surface bound physiosorbed species, or with the formation of

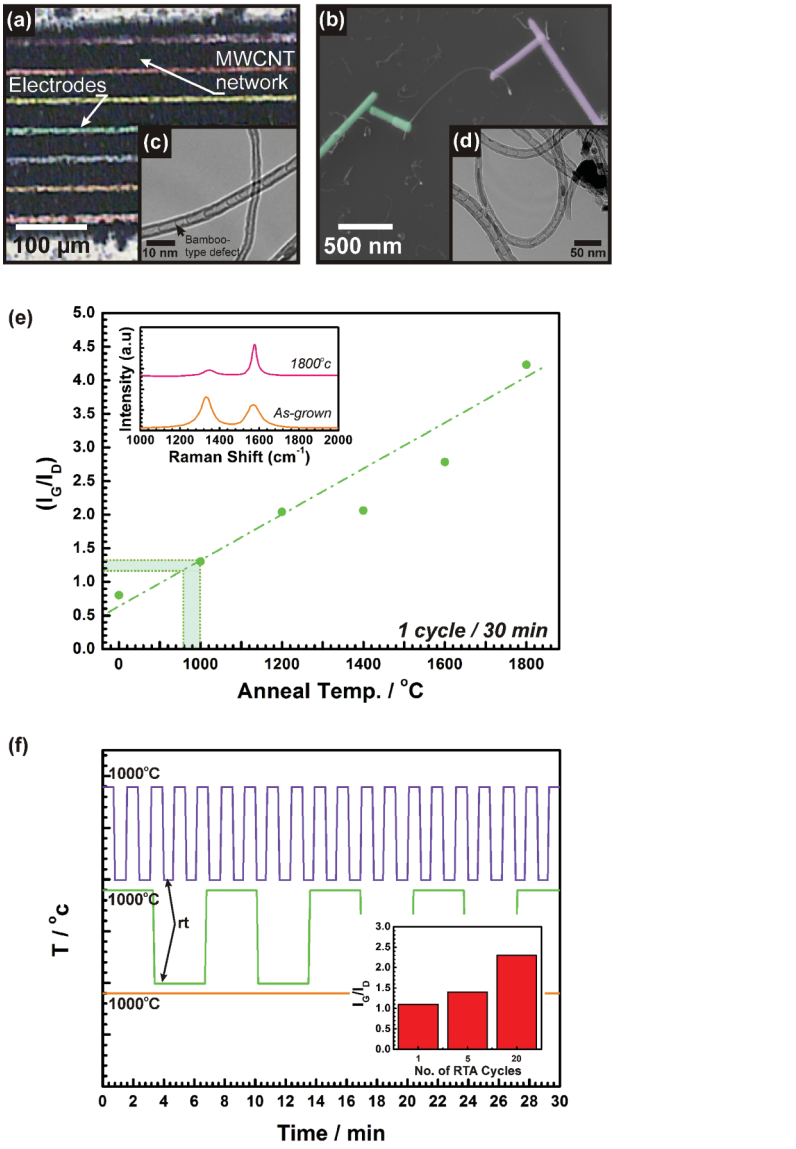

Figure 1. Optical and scanning electron micrograph of a typical fabricated (false colored) **(a)** network sample and **(b)** An individual FIB connected MWCNT (Scale bars: 100 µm and 500 nm, respectively). **(c, d)** HR-TEM micrographs of an as-grown and pulsed RTA processed samples. As-grown MWCNTs have approx. 200 defects/µm and RTA processed samples around 42 defects/µm. **(e)** Micro-Raman I_G/I_D ratio dependency on RTA (1 cycle/30 min) temperature. *Insert:* Typical Raman spectra of the as-grown and RTA processed samples [14]. **(f)** RTA processing thermal profiles. *rt* denotes room temperature. *Insert:* I_G/I_D ratio enhancement, at 1000 K, through thermal pulsing. 20 cycles increased the I_G/I_D by a factor of two.

inter-tube junctions by graphitization, for example. In the case of an increase in the number of graphitized CNT junctions, conductivity enhancement is achieved through increased network connectivity, and it is therefore reasonable that there would be negligible enhancement in the conductivity of individual MWCNTs following the RTA processing. Thus, individual RTA processed MWCNTs and RTA processed MWCNT networks must be considered.

In any case, a good understanding of the association between thermal treatments and conductivity is important in engineering high quality nanostructured networks.

Dai et al. (15) found that the most structurally perfect nanotubes have conductivities an order of magnitude larger than MWCNTs with high defect densities. Endo et al. reported significant structural alteration in highly-defective "stacked cup" carbon nanofibres and a resulting near monotonic reduction in resistivity when thermally treated up to ~3000 K (16). This variation was attributed to increased levels of connectivity throughout the networks, especially between the outer surfaces of the carbon nanofibers (1). Ebbesen et al. (16) evidenced for arc-discharge MWCNTs thermally annealed at 3120 K, both metallic and nonmetallic behavior inferring that different CNT geometries play a profound role in determining the electronic behavior (16), highlighting the necessity for further study on the effects of thermal treatments.

Experimental

MWCNTs were prepared by Sm-Co liquid catalyst microwave plasma assisted CVD at 650°C. The detailed synthesis procedure is described elsewhere (12). Samples were vacuum spark-annealed at 2070 K (570 Ks^{-1}) at 5.7 mbar. High-resolution tunneling electron microscopy (HR-TEM, Hitachi H-7100) was employed to quantify the degree of defectiveness of the as-grown and RTA processed samples. As-grown MWCNTs had defect densities of approximately 200–500 μm^{-1} (Figure 1a).

Micro-electrodes (with a separation of 25 μm) were photolithographically defined on 200-nm-thermally oxidized n^+ doped Si substrates. A 500 nm Au film was then magnetron sputtered (10^{-7} mbar base pressure) to form the micro-electrode structures. The as-grown and RTA processed MWCNTs, approximately 5–15 μm in length and 10–30 nm in diameter, evaluated by high-resolution scanning electron microscopy (SEM), were dispersed in separate solutions of isopropanol and deionized water and were filtered (Millipore) and centrifuged to remove large bundles, agglomerates, and other undesirable carbonaceous species. Samples were then agitated for 1 hour and allowed to settle for 48 hours to separate off residual heavy particles (such as nondispersed MWCNTs and freed catalyst particles). The solution was then drop-cast onto the center of the Au contacts. A detailed overview of this drop-casting process can be found in (13). Network MWCNT samples were fabricated by dielectrophoresis via the application of an alternating current square-wave (16 $V_{p\text{-}p}$/1 MHz). Figure 1a shows a final MWCNT network sample. From this configuration the differential conductivity of the as-grown and RTA processed MWCNT networks was measured. This structure also permitted back-gating characterisation using the underlying highly doped Si support as a back gate.

To compare the level of thermal enhancement between individual MWCNTs and the MWCNT networks, low-density MWCNT solutions were similarly dispersed by drop casting onto thermally oxidized Si substrates. Individual MWCNTs were then located by SEM, mapped and contacted with Al nano-electrodes fabricated by focus ion beam (FIB) milling (Figure 1b).

In our previous work various annealing temperatures were investigated via micro-Raman spectroscopy. Figures 1e and f summarize the data extrapolated from (14). We note an increase of *ca.* 4.25 in the I_G/I_D ratio, occurring at 2070 K for a single thermal cycle over 30 minutes. The effect of rapid multipulse annealing compared with more traditional annealing (i.e., single pulse) was also investigated. It was found that single pulse annealing (more typical of standard slow thermal processing) resulted in small I_G/I_D enhancement compared to our RTA multipulse processing which employed high thermal pulse rates (Figure 1f). At 1000 K, for one thermal cycle the I_G/I_D ratio increased to ~ 1.1 while

for 20 cycles it increased to $\sim$ 2.3 (thermal profiles illustrated in Figure 1f). Herein samples were prepared by using the RTA processing and were annealed at 1800 K/20 cycles.

Transport measurements where performed in a high vacuum chamber (base pressure $\sim 10^{-7}$ mbar) fitted with a thermally adjustable stage (297–77 K) and *in-situ* electrical probes connected to LABVIEW controlled Keithley 4200 SCS source-meters, with sub-pA resolution.

All contacts were deposited *after* RTA processing. Throughout this study, as-grown and annealed samples represent separate samples, *not* the same sample, before and after RTA processing. This is because thermal treatments are known to adjust the interfacial resistance between the MWCNTs and the electrode, thereby altering the measured conductivity. Thus, by employing separate samples such effects have been negated.

Results and Discussion

Figure 2 shows a typical room temperature *I-V* characteristic of an as-grown (dashed line) and RTA processed (solid line) sample. The insert shows an optical and SEM micrograph of a typical micro-electrode structure. Figure 3a illustrates the temperature (T) dependence of the differential conductance of an as-grown network (S1), RTA processed network (S2), and an RTA processed individual MWCNT (S3). We observed, as reported by Dai et al. (15), that the most graphitic MWCNTs (as indicated by our previous Raman studies) have the highest conductivities, of the order of 4.7 times that of the as-grown, defect-rich samples. Here, however, we note a striking consistency between the enhancement of the conductivity and the enhancement of the I_G/I_D ratio. This result indicates that researchers may, tentatively, use the (I_G/I_D) ratio enhancement as a rapid, noninvasive, and indirect means of estimating conductivity enhancement in MWCNTs (and potentially other discrete carbon nanostructures) following RTA processing.

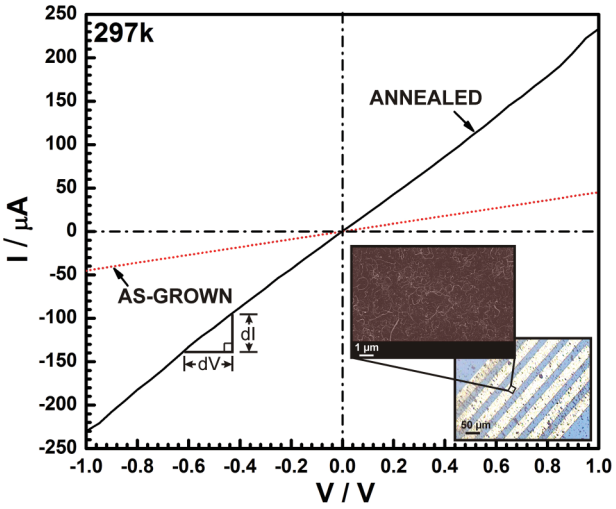

Figure 2. DC room temperature I-V characteristic of the as-grown and RTA processed (ANNEALED) MWCNT networks. Insert: Optical and scanning electron micrographs of a MWCNT network sample. Scale bars: 50 µm and 1 µm, respectively.

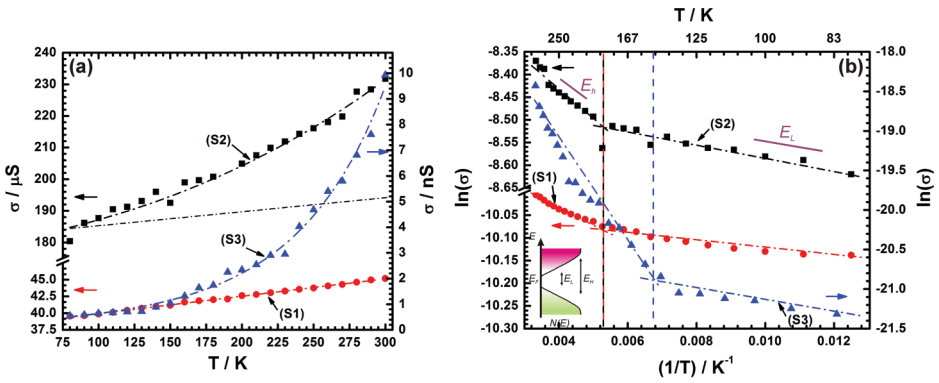

Figure 3. **(a)** Transport characteristics Arrhenius plot for the network (S1), and RTA process samples; (S2) MWCNT bundle network and (S3) individual MWCNT. The dot-dash line in (a) is plotted as a guide to emphasize the enhanced semiconducting behavior enhancement between samples (S1) and (S2) as a result of the annealing process. **(b)** Conductance Vs. temperature Arrhenius plot for an individual annealed, as-grown network and RTA processed networks have room temperature band gaps of 107, 6.17 and 11.26 meV, respectively. Saturation transition temperatures of 185.4 K and 144.6 K are noted for the network and individual MWCNT samples, respectively. No notable shift in the saturation transition temperature is observed for the as-grown network (S1) and RTA processed network (S2). *Insert:* Schematic representation of the simplified energy band structure of the MWCNTs with band tails with possible intermediate localized states.

All samples showed an increase in conductivity with increasing temperature, tending toward a saturation conductivity. Langer et al. (17) reported a similar trend and argued that the effect was due to weak localization in a disordered two-dimensional conductor. The observed decrease in conductivity with decreasing temperature may also be in part associated with a Peierls type transition (16). The as-grown network, RTA processed network, and RTA individual MWCNT samples showed saturation conductivities of 45.4 μS, 231.7 μS, and 9.8 nS, respectively. The pronounced increase in conductivity of the network samples compared with the individual MWCNTs may also in part be attributed to CNT-CNT junction recrystallization forming reduced resistance cross-junctions as well as removal of charge-doping surface bound species. Satishkumar et al. (18) reported the formation of CNT-CNT "Y"-junctions during pyrolysis at 1273 K of an Ar/H_2 mixture bubbled through thiophene employing nickelocene. Further investigations are underway to define this effect further.

Both the network and individual RTA processed samples displayed a thermally enhanced, weakly semiconducting behavior, evidenced by higher conductivities at elevated temperatures and a parabolic variation in differential conductivity with temperature. This trend was most significant in the individual MWCNT samples. Thermal stimulation to increase charge carrier concentrations is a characteristic feature known to enhance electrical conduction in semiconductors and not in metals. From our conduction measurements it is evident that the measured conductance follows an Arrhenius-type behavior, a result indicative of thermally activated charge transport across a band gap, E_g, in semiconducting materials (19). We can estimate the carrier concentration from equation (1),

$$n = N \exp\left(\frac{-(E_c - E_f)}{k_b T}\right) \Rightarrow \sigma = \sigma_o \exp\left(\frac{-E_g}{2K_b T}\right) \quad (1)$$

where n is the electron concentration; N is the effective density of states in the conduction band; E_c and E_f are the conduction band edge and Fermi level, respectively; k_b is Boltzmann's constant; and T is the absolute temperature.

By expressing (1) in terms of conductivity, σ, and the saturation conductivity at high temperature, σ_0, and fitting our data from Figures 3a and b it is possible to estimate the associated thermally induced variation in band gap. From Figure 3b it is clear that there exists two distinct regimes, suggesting a nonmonotonous nontrivial density of states (20), defined by a transition at a temperature T^*. Here T^* refers to the transition temperature associated with the shift to thermally activated transport. High- ($T>T^*$, HT) and low-temperature ($T<T^*$, LT) regime band gaps are denoted E_H and E_L, respectively (as illustrated in the insert of Figure 3b). For the MWCNT network and individual RTA samples $T^* = 185.4$ and 144.6 K, respectively. The observed T^* remain fixed after pulsed RTA processing. From equation (1) we find $E_{gH/gL} \approx 6.17/1.37$ meV (as-grown) and 11.26/2.52 meV (RTA). The pulsed RTA processing increased both the HT and LT band gaps by approximately 1.8 times that of the as-grown MWCNTs. The induced band gap widening, $\Delta E_{gH/gL}$, was approximately 5.09/1.15 meV. Individual RTA MWCNT samples showed $E_{gH/gL} = 107/13$ meV. Individual MWCNTs had high temperature ($T>T^*$) energy gaps four times that of ambient thermal stimulation (25 meV at 300 K) and it is therefore reasonable to formulate E_{gH} as the apparent energy gap between the conduction and valance band tail states (20).

Previous reports (21) showed that charge carrier transport principally occurs in the outermost shell. For incommensurate graphene cylinders the energy gap scales with diameter as $E_g = (2\gamma_0 a_{c\text{-}c}/d)$ where γ_0 is the C–C tight-binding overlap energy, a_{c-c} the nearest neighbor C–C distance (0.142 nm), and d is the tube diameter (22). On application of this equation we find that $E_g = 35.5-11.8$ meV, which is consistent with our measurements.

However, the underlying mechanism for the observed band gap widening is still unclear. Thermally induced strain may account for this. In metallic SWCNTs minor strains induce band gap widening. This band gap, between the first van Hove singularities, under the uniaxial stress can be expressed by (23,24):

$$E_g \approx 3t_o\,(1+\nu)\,\gamma \tag{2}$$

where t_0 is the hopping parameter/C-C tight-binding overlap integral (24), ν is Poisson's ratio, and γ is the tube elongation (25). The maximized value of (2), $|\Delta E_g/\Delta\gamma|$, gives $3t_o(1+\upsilon) \approx 100\text{meV}/\%$ (24). The thermally induced strain within the nanotube is given by $\Delta\gamma = \alpha.\Delta T$, where ΔT is the change in temperature (which equates to the annealing temperature, 2000 K), and α is the thermal expansion coefficient ($\approx 1.3 \times 10^{-5}/\text{K}$ [26]); we find that $\Delta E_g = 2.6$ meV, which is in reasonable agreement with the measured network sample data. Individual MWCNTs samples deviate from this model somewhat due to substantially increased axial strains imparted by the mechanical pinning of the probe electrodes.

To further investigate the enhanced semiconductivity inferred from Figure 3, gating potentials (V_g) were applied to the underlying degenerately doped Si substrate. Figures 4a and b show the measured gating transfer characteristics. The plot in Figure 4a details the I_{sd}-V_{sd} response of two *different* samples; an annealed and as-grown sample. These two samples have different MWNT densities and therefore different σ values, an unavoidable effect of the fabrication process. In this instance the as-grown sample has a higher network density than the annealed sample. Consequently the as-grown MWNCNTs had a higher σ. Note that that the annealing process *did not* reduce σ. This variation in σ is attributed to

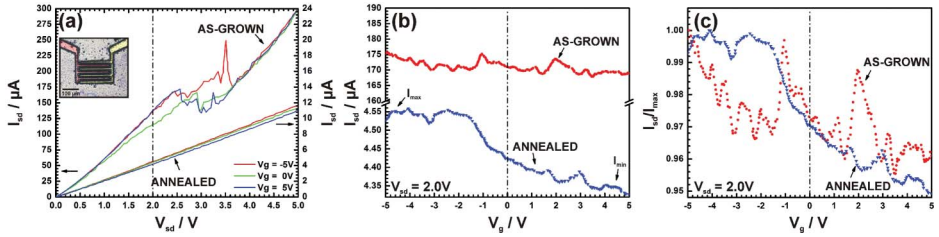

Figure 4. Room temperature transfer characteristics of **(a)** as-grown (network density = A) and **(b)** RTA processed sample (network density = B), where B<A, based on the fabricated back-gated network MWCNT-FET structures. *Insert*: Optical micrograph of a typical MWCNT network device. **(c)** Network density independent normalized transfer characteristics. Weakly *p*-type semiconducting behavior of a pulsed RTA processed sample (▼). As-grown samples (●) show negligible gating behavior (nominally metallic) under identical biasing conditions ($V_{sd} = 2.0$V).

variation in network density. Comparative σ data have not been extracted from Figure 4a as a result, and we have only extracted comparative gating performance of the two devices (Figures 4b and c).

The as-grown samples behaved in a purely metallic fashion where the applied gate bias did not notably modulate the source-drain current, I_{sd}, compared with the underlying noise. The transport characteristics of the as-grown samples were rather noisy (Figure 4c), a result of the high defect density (and therefore scatter sites) within the MWCNTs. The measured source-drain currents (I_{sd}) in Figure 4c have been normalized to the maximum current (I_{max}) measured during gating to account for variations in MWCNT network densities (and hence σ variations) between RTA and as-grown samples, as discussed previously. The number of interconnecting MWCNTS varies between fabricated samples, as evidenced by the unexpectedly large I_{sd} of the as-grown sample compared to the RTA processed sample, in Figure 4a. Normalizing the data to the maximum observed current (I_{max}) removes this effect.

The reduced signal noise in the annealed sample (Figure 4c) is due to the reduction in the number of scattering sites following pulsed graphitization and ensures that the transfer characteristics are not flooded by noise. As predicted from the temperature dependence of the differential conductivity measurements at zero source-drain potential, $dI_{sd}/dV_{sd}|_{Vsd=0}$, the RTA sample did demonstrate weakly *p*-type semiconducting behavior compared with the as-grown sample, under identical bias conditions. But what gives rise to the *p*-type gating behavior? The formation of a Schottky barrier at electrode-MWCNT interface plays the dominate role (27). Band-widening results in an enhancement of the Schottky barrier at the interface, as schematically illustrated in Figure 5. The observed *p*-type behavior is consistent with Pd contacted CNT-FETs (27). The *p*-type behavior here contradicts the reported characteristics of directly N_2 doped MWCNTs (*n*-type) (28). Thus, negligible structural incorporation of the compartmentalized N_2 (within the source bamboo-defect rich MWCNTs) occurs during the RTA processing and that variation in conductivity is not a result of weakly surface bound physisorbed N_2 liberation. The enhanced gating behavior is principally attributed to the thermally induced strain increasing the band gap which enhances the MWCNT-Au interfacial Schottky barrier. This effect that was further enhanced by a notable reduction in electronic noise achieved through removal of scattering sites through thermally stimulated graphitization. We propose that this effect occurs specifically in the outermost shell and is enhanced through a pulsed annealing treatment; it was evidenced by the consistency of our measured data and the band gap-diameter relationship.

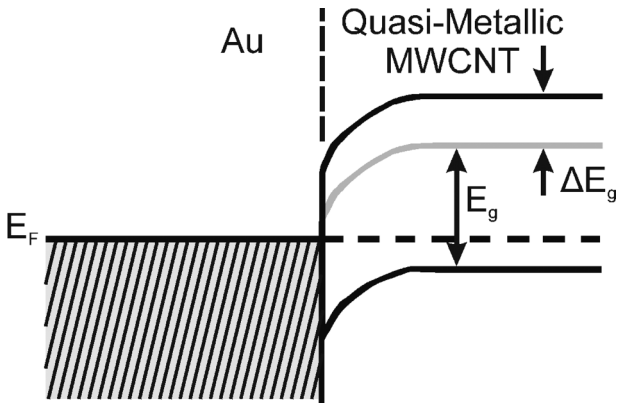

Figure 5. Schematic diagram of *p*-type Schottky barrier at the Au-MWCNT interface. Thermally induced band gap opening gives rise to the enhanced gating behavior.

Data were further corroborated by considering the thermally induced strain as a model system to account for the variation in channel conductivity.

Conclusion

Here we have demonstrated a simple postsynthesis route towards simultaneous conductivity and semiconducting behavior enhancement. The temperature dependence of the differential conductivity of as-grown and pulsed RTA processed networks and individual MWCNTs have been compared. RTA processing increases the degree of crystallinity of the MWCNTs graphitic lattice as opposed to simply increasing the degree of connectivity within the MWCNT network. We found that the increasingly crystalline MWCNTs in both networks and individual samples, enhanced by the pulsed RTA postprocessing, not only exhibit higher conductivities (up to five times larger) compared with the defective, as-grown MWCNT counterparts but also are a weak *p*-type semiconductivity at room temperature attributed to thermally induced strains opening the nonnegligible band gap. Measured data showed good agreement with modeled estimates typically employed for SWCNTs.

Funding

This project is financially sponsored by National Science Council (grant no. NSC 95-2112-M-036-001-MY2) and Tatung University (grant no. B97-O02-055). M. T. Cole thanks the Schiff Studentship, Cambridge University, for generous financial support.

References

1. Endo, M., Kim, Y.A., Hayashi, T., Yanagisawa, T., Muramatsu, H., Ezaka, M., Terrones, H., Terrones, M., and Dresselhaus, M.S. (2003) *Carbon*, 41(10): 1941.
2. Krstic, V., Muster, J., Duesberg, G.S., Philipp, G., Burghard, M., and Roth, S. (2000) *Synth. Met.*, 110(3): 245.
3. Skakalova, V., Kaiser, A.B., Dettlaff, U., Arstila, K., Krasheninnikov, A.V., Keinonen, J., and Roth, S. (2008) *Physica Status Solidi B-Basic Solid State Physics*, 245(10): 2280.
4. Qu, L. and Dai, L. (2007) *Adv. Mater.*, 19(22): 3844.

5. Chongwu, Z., Jing, K., and Hongjie, D. (2000) *Appl. Phys. Lett*., 76(12): 1597.
6. Javey, A., Guo, J., Wang, Q., Lundstrom, M., and Dai, H.J. (2003) *Nature*, 424(6949): 654.
7. Xiaolei, L., Chenglung, L., Chongwu, Z., and Jie, H. (2001) *Appl. Phys. Lett*., 79(20): 3329.
8. Ajayan, P.M., Schadler, L.S., Giannaris, C., and Rubio, A. (2000) *Adv. Mater*., 12(10): 750.
9. Ramasubramaniam, R., Chen, J., and Liu, H.Y. (2003) *Appl. Phys. Lett*., 83(14): 2928.
10. Shaffer, M.S.P. and Windle, A.H. (1999) *Adv. Mater*., 11(11): 937.
11. Reyes-Reyes, M., Grobert, N., Kamalakaran, R., Seeger, T., Golberg, D., Ruhle, M., Bando, Y., Terrones, H., and Terrones, M. (2004) *Chem. Phys. Lett*., 396(1–3): 167.
12. Tsai, J.T.H. and Chen, K.H. (2005) *Int. J. Nanosci*., 4(4): 431.
13. Tsai, J.T.H., Lu, C.-C., and Li, J.G. (2010) *J. Exp. Nanosci*., 5(4): 7.
14. Tsai, J.T.H. and Tseng, A.A. (2009) *J. Exp. Nanosci*., 4(1): 87.
15. Dai, H.J., Wong, E.W., and Lieber, C.M. (1996) *Science*, 272(5261): 523.
16. Ebbesen, T.W., Lezec, H.J., Hiura, H., Bennett, J.W., Ghaemi, H.F., and Thio, T. (1996) *Nature*, 382(6586): 54.
17. Langer, L., Bayot, V., Grivei, E., Issi, J.P., Heremans, J.P., Olk, C.H., Stockman, L., VanHaesendonck, C., and Bruynseraede, Y. (1996) *Phys. Rev. Lett*., 76(3): 479.
18. Satishkumar, B.C., Thomas, P.J., Govindaraj, A., and Rao, C.N.R (2000) *Appl. Phys. Lett*., 77(16): 2530.
19. Agrawal, S., Raghuveer, M.S., Li, H., and Ramanath, G. (2007) *Appl. Phys. Lett*., 90(19): 193104.
20. Eda, G., Mattevi, C., Yamaguchi, H., Kim, H., and Chhowalla, M. (2009) *J. Phys. Chem. C*, 113(35): 15768.
21. Bachtold, A., Strunk, C., Salvetat, J.P., Bonard, J.M., Forro, L., Nussbaumer, T., and Schonenberger, C. (1999) *Nature*, 397(6721): 673.
22. Wildoer, J.W.G., Venema, L.C., Rinzler, A.G., Smalley, R.E., and Dekker, C. (1998) *Nature*, 391(6662): 59.
23. Okubo, S., Okazaki, T., Kishi, N., Joung, S.K., Nakanishi, T., Okada, S., and Iijima, S. (2009) *J. Phys. Chem. C*, 113(2): 571.
24. Minot, E.D., Yaish, Y., Sazonova, V., Ji-Yong, P., Brink, M., and McEuen, P.L. (2003) *Phys. Rev. Lett*., 90(15): 156401/1.
25. Liu, Y. and Jie, H. (2000) *Phys. Rev. Lett*., 85(1): 154.
26. Ge, J.J., Hou, H.Q., Li, Q., Graham, M.J., Greiner, A., Reneker, D.H., Harris, F.W., and Cheng, S.Z.D. (2004) *JACS*, 126(48): 15754.
27. Yang, M.H., Teo, K.B.K., Milne, W.I., and Hasko, D.G. (2005) *Appl. Phys. Lett*., 87(25).
28. Xiao, K., Liu, Y.Q., Hu, P.A., Yu, G., Sun, Y.M., and Zhu, D.B. (2005) *JACS*, 127(24): 8614.